Clustering and selection of hurricane wind records using a machine learning approach

Xinlong Du[1], Jerome F. Hajjar[2], Robert Bailey Bond[3], Pu Ren[4] and Hao Sun[5]

[1]Graduate Research Assistant, Department of Civil and Environmental Engineering, Northeastern University, Boston, MA 02115, USA. Email: du.xinl@northeastern.edu

[2]CDM Smith Professor and Chair, Department of Civil and Environmental Engineering, Northeastern University, Boston, MA 02115, USA. Email: jf.hajjar@northeastern.edu

[3]Graduate Research Assistant, Department of Civil and Environmental Engineering, Northeastern University, Boston, MA 02115, USA. Email: bond.rob@northeastern.edu

[4]Graduate Research Assistant, Department of Civil and Environmental Engineering, Northeastern University, Boston, MA 02115, USA. Email: ren.pu@northeastern.edu

[5]Associate Professor, Gaoling School of Artificial Intelligence, Renmin University of China, Beijing, China. Email: haosun@ruc.edu.cn

ABSTRACT

In wind engineering, to accurately estimate the nonlinear dynamic response of structures while considering uncertainties of hurricanes, a suite of wind records representing the hurricane hazards of a given location is of great interest. Such a suite generally consists of a large number of hurricane wind records, which may lead to highly computational cost for structural analysis. To reduce the computational demand while still preserving the accuracy of the uncertainty quantification process, this paper proposes a machine learning approach to select a representative subset of all collected hurricane wind records for a location. First, hurricane wind records, which are expressed as time series with information that includes both wind speed and direction, are collected from a synthetic hurricane catalog. The high-dimensional hurricane wind records are then compressed into a set of low-dimensional latent feature vectors using an artificial neural network, designated as an autoencoder. The latent feature vectors represent the important patterns of wind records such as duration, magnitude and the changing of wind speeds and directions over time. The wind records are then clustered by applying the k-means algorithm on the latent features, and a subset of records is selected from each cluster. The wind records selected from each cluster are those whose latent feature points are closest to the centroid of all latent feature points in that cluster. In order to do regional analysis

while taking into account that the hurricane wind records are site-specific, this paper suggests that a region can be discretized into a set of grids, with the proposed hurricane selection approach applied to each grid. This procedure is demonstrated using Massachusetts as a testbed.

Keywords: hurricane selection, time series clustering, autoencoder, k-means, uncertainty quantification, regional analysis, wind direction

1. Introduction

Nonlinear dynamic analysis is increasingly being considered in wind design of buildings and other structures as performance-based design becomes an increasingly popular option (ASCE, 2019), where controlled inelastic deformations are allowed under strong winds (Wang and Wu, 2022). In the fully probabilistic performance-based hurricane engineering framework (Barbato et al., 2013), fragility curves of structures are commonly adopted to do probabilistic damage assessment. Strength limit states of structures usually involve nonlinear behavior that is then integrated into the predictions of likelihood of damage that is offered through fragility analysis. Fragility functions are defined as the failure probability of a structure conditional on the intensity measure of hazards, including hurricanes in this work. If only the failure probability or fragility is of interest for a hurricane event (i.e., at the end of the loading time history) instead of for a certain time interval within the hurricane duration, the uncertainties in the loading time histories can be accounted for through running a series of nonlinear dynamic analysis with a suite of hurricane wind records. The hurricane wind records should include time histories that incorporate the wind directions as well as wind speeds, because the changing of wind directions during hurricanes has significant effects on the structural response. Consequently, the wind records in this research are time series of both wind speed and direction. To develop accurate fragility curves, the structures should be analyzed with a suite of hurricane wind records that can cover the record-to-record uncertainties in the changing of wind speeds and directions within the hurricane durations. A large amount of hurricane wind records can be collected for a location considering the existing historical and synthetic hurricanes (ASCE, 2016; Vickery et al., 2010; Vickery et al., 2009b; Vickery et al., 2009c). However, it is challenging to run nonlinear dynamic analysis for all of the collected hurricane records due to the high computational demand of finite element analysis of structures; thus, a minimum number of hurricane records should be selected to represent the uncertainties in all of the collected hurricane records.

In prior work, Li (2005) and Li and Ellingwood (2006) developed hurricane fragility curves for wood-frame residential construction with a simplified limit state function, where the nonlinear and dynamic effects are neglected. Cui and Caracoglia (2015) carried out fragility analysis on tall buildings only for the serviceability limit state, so frequency domain analysis is adopted, and duration and nonstationary effects of hurricanes cannot be considered. In order to avoid performing structural analysis for long durations of windstorms, the dynamic shakedown method was utilized by researchers to model the inelastic behavior of buildings; however, this method assumes small displacement and deformation, so the buckling effects of structures like electrical transmission towers cannot be accounted for (Chuang and Spence, 2019, 2020; Tabbuso et al., 2016). Other researchers tried to develop hurricane fragility curves using nonlinear dynamic analysis only for a fixed time interval with a constant wind direction. For example, Hallowell et al. (2018)

used wind records with 1-hour time intervals, while Ma et al. (2021) used wind records with 2-minute time intervals. The fragility developed for this certain time interval cannot represent the fragility for a whole hurricane because of dynamic effects, yielding and changes in wind speeds and directions. Of course, one can discretize the hurricane duration into a series of short time intervals and apply the developed fragility curves to each short time interval; however, the failure probabilities within those short time intervals are correlated (Der Kiureghian, 2005; Kim et al., 2019; Straub et al., 2020). This correlation is difficult to quantify from the view of time-variant reliability and is not considered by the above authors. Given the limitations of the previous research, this paper considers the failure probability for a hurricane event instead of a certain time interval during a hurricane and tries to select hurricane wind records that can account for the record-to-record uncertainties in hurricanes. The selected wind records can be used to estimate failure probabilities of structures with nonlinear time history analysis. Through this way it is no longer needed to estimate the correlations of failure probabilities in the short time intervals within a hurricane.

In performance-based earthquake engineering (Moehle and Deierlein, 2004), a probabilistic framework has been proposed to integrate seismic hazard analysis and structural damage analysis, where a suite of ground motions are adopted to represent the uncertainties in earthquake ground motions. Ground motion selection has been widely studied in the literature (Baker and Lee, 2018; Bojórquez et al., 2013; Du and Padgett, 2021; Jayaram et al., 2011; Naeim et al., 2004). Some generally used ground motions suites are the SAC (Somerville et al., 1997) records, LMSR (Krawinkler et al., 2003) records, and FEMA-P695 records (FEMA, 2009). Recently, machine learning approaches have also been introduced to ground motion selection, where a reduced number of ground motions are obtained through clustering of a large number of ground motions (Bond et al., 2022; Kim et al., 2021; Zhang et al., 2020). However, there is no similar research in the literature for selection of hurricane wind records. There are two instances of prior research that consider uncertainties in hurricane wind hazards using a set of wind records, but they do not use a selection procedure. Vickery et al. (2006) studied hurricane fragility curves for building envelope components that were developed in the Hazus-MH software by comparing the wind pressure demand and the capacity of the envelope components. The record-to-record uncertainties of hurricane wind speeds were accounted for through the use of a 20,000-year simulation of hurricanes created by employing the hurricane model described by Vickery et al. (2000a) and Vickery et al. (2000b). The simulated hurricanes inherently incorporated many of the duration effects associated with the changes in wind speed and direction which accompany hurricane winds. Joyner and Sasani (2018) developed fragility curves for the windborne debris damage of building glazing, where eight hurricanes that made landfall in the U.S. in the last 10 years were adopted. Uncertainties in the record-to-record variability for different hurricanes were accounted for by employing the eight hurricane records in the damage analysis. Vickery et al. (2006) used all hurricanes in

101 the 20,000-year simulation, which may address the uncertainties in hurricanes, but is not suitable for
102 nonlinear dynamic analysis considering the computational demand. On the contrary, Joyner and Sasani
103 (2018) only used eight hurricanes without an analysis of the hazard uncertainties, which may not be able to
104 represent the uncertainties in hurricanes for a specific location.

105 This paper proposes a procedure to select a suite of hurricane wind records that can be used for performance-
106 based design and fragility analysis. The wind speed and direction records for a location are collected from
107 a synthetic hurricane catalog (Liu, 2014) with some preprocessing, after which the collected wind records
108 have durations that are short enough to make a nonlinear time history analysis feasible. The collected wind
109 records are then compressed into low-dimensional latent feature vectors using a neural network designated
110 as an autoencoder (Aggarwal, 2018), so that it is easier to measure similarity of different wind records and
111 apply the standard clustering algorithms such as the k-means algorithm (Aggarwal et al., 2001; Shalev-
112 Shwartz and Ben-David, 2014). Autoencoder is an artificial neural network in which the input and output
113 layers have the same number of neurons, while the number of neurons in the middle is constricted. The
114 training algorithm tries to reconstruct the input data in the output layer; however, this reconstruction is not
115 exact because the neurons in the middle only carry a reduced representation of the input data. The data held
116 by the neurons in the middle (i.e., the low dimensional vectors compared to the input and output layer) are
117 called latent features, to which the clustering algorithm is applied. This means that only important
118 information in the wind records is preserved for clustering. The latent features representing hurricane wind
119 records are then clustered into several groups using the conventional k-means algorithm (Shalev-Shwartz
120 and Ben-David, 2014). Finally, only a few hurricane wind records are selected from each cluster for fragility
121 development or design checks, which significantly reduces the number of required time history analyses,
122 while still ensuring that the uncertainties of different hurricanes are covered with a limited number of wind
123 records. Since the properties of hurricanes for different locations have significant differences, a hazard map
124 can be developed for hurricane wind records so that users are able to choose appropriate records for their
125 locations of interest. As an example, the Commonwealth of Massachusetts has been divided into 92 grids
126 and a suite of hurricane wind records has been selected for each grid using the proposed hurricane selection
127 approach. To demonstrate the usefulness and effectiveness of the selected wind records, they have been
128 adopted to develop fragility curves for electrical transmissions towers in Massachusetts, which can be found
129 in Du et al. (2022) and Du and Hajjar (2022).

130 2. Hurricane simulation

131 Synthetic hurricanes are widely used for risk analysis and structural design in wind engineering, which
132 evolved from the single site probabilistic model (Russell, 1971) to Vickery's hurricane track model

(Vickery et al., 2000a). For example, ASCE 7 has adopted the hurricane track model when generating the wind hazard maps (ASCE, 2016). This research also uses a 10,000 year synthetic hurricane catalog developed by Liu (2014) for the Atlantic basin based on Vickery's hurricane track model, which consists of a hurricane genesis model, a track model, an central pressure model, a decay model and a boundary layer model. The temporal and spatial evolution of thousands of hurricanes from emergence to dissipation was modeled using the Monte Carlo method. The HURDAT database (Jarvinen et al., 1984) for historical storms was adopted for building the hurricane model through regression and calibrating the simulated results. In this simulation, the state of a hurricane can be determined with 7 parameters: the hurricane eye's latitude and longitude, storm translation speed, storm heading angle, storm central pressure, radius to maximum winds (describing storm size), and Holland's radial pressure profile parameter (i.e., the Holland B parameter (Holland, 1980)). These parameters are updated at each 6-hour point. As suggested by Vickery et al. (2000a), linear interpolation is performed within each 6-hour interval, which results in 10-min updates of the parameters as used in Vickery et al. (2009c). Examples of the simulated hurricane tracks are shown in Fig. 1. In this research, the gradient wind speeds are calculated by employing Georgiou's model (Georgiou, 1985), which gives the 10-min sustained wind speeds at 500 m to 2000 m above the ground surface (Cui and Caracoglia, 2019; Pei et al., 2014, 2018). An example of the calculated gradient wind field is shown in Fig. 2.

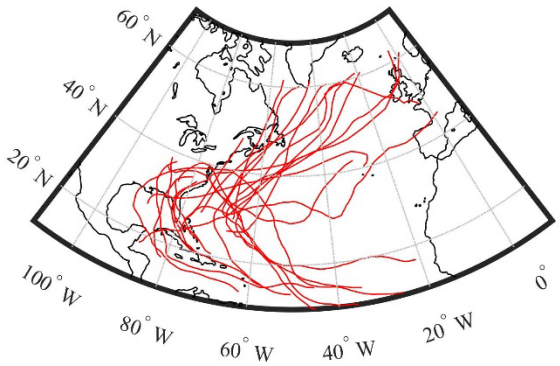

Fig. 1. Examples of the simulated hurricane tracks

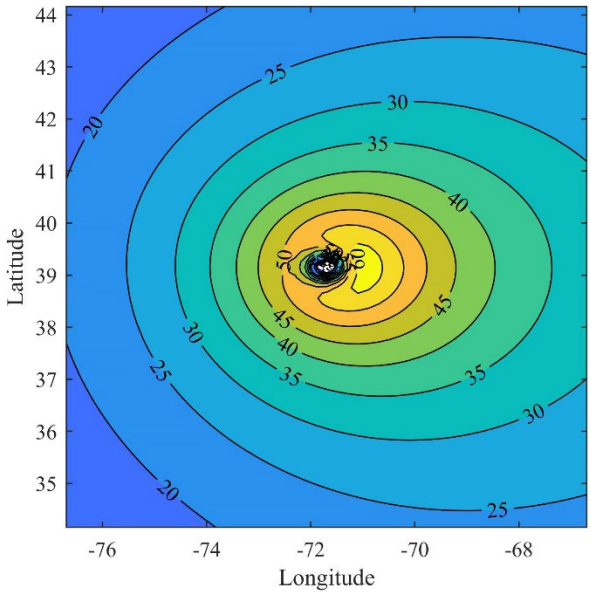

Fig. 2. Example of hurricane gradient wind field (m/s)

The obtained hurricane gradient wind speeds V_g need to be converted to surface wind speeds V_{10} (10 m above the ground or water) for wind force calculation on structures. The reduction factor V_g/V_{10} over water proposed by Batts et al. is used in this research (Batts et al., 1980; Vickery et al., 2009a). A sea-land transition factor obtained from the model given in Simiu and Scanlan (1996) is then utilized to calculate the surface wind over land (open terrain with surface roughness $z_0 = 0.03\,m$) from the surface wind over water ($z_0 = 0.0013\,m$). In addition, the surface wind speed over land approaches the fully transitioned value asymptotically over a fetch distance as the wind moves from sea to land; therefore, the transition function proposed in Vickery et al. (2009b) is employed here, which defines the percentage of the sea-land transition as a function of the fetch distance. With the methods discussed in this section, the time series of the 10-min sustained wind speeds at 10 m height and the corresponding wind directions at a location of interest (assuming open terrain) during a hurricane may be obtained.

3. Hurricane wind records collection and preprocess

ASCE 7 wind hazard maps display wind speeds with a certain mean recurrence interval (MRI) for the entire U.S., including hurricane prone regions (ASCE, 2016). However, much information regarding hurricane winds is omitted in the ASCE 7 wind hazard maps, such as the variation of wind speeds and directions during a hurricane, and the durations of hurricane winds. This kind of information, which are contained in the time series of hurricane wind speeds and directions, are critical for structural response estimation and risk analysis. Thus, in this section, a number of hurricane wind speed and direction records are collected

for a location of interest. In order to collect hurricane wind records for a region, the region is first discretized into a series of grids and then hurricane wind records are collected for each grid.

3.1. Wind records for a location of interest

A location in Massachusetts with latitude 41.7 and longitude -70.1 is used as an example in this section. Wind records are collected for this specific location from 10,000-year synthetic hurricanes developed by Liu (2014). Examples of the collected 10-min sustained wind speed and wind direction records at the location of interest are shown in Fig. 3 to Fig. 5 with the corresponding hurricane tracks. It is seen in Fig. 3(a), Fig. 4(a) and Fig. 5(a) that the hurricane eye usually moves thousands of miles from a hurricane's genesis to dissipation. It is reasonable to assume that the wind speed induced by a hurricane that is very far away is relatively small and can be neglected. Therefore, as suggested by Vickery et al. (2009c), hurricane winds are considered only when the location of interest is within 250 km of the hurricane eye (see the blue circles in Fig. 3 to Fig. 5). This limit on distance also provides a limit for the durations of the hurricane wind records. Figure 3(c), Fig. 4(c) and Fig. 5(c) illustrate the absolute values of the wind speeds and the wind directions in a polar coordinate system, while Fig. 3(d), Fig. 4(d) and Fig. 5(d) illustrate the hurricane wind speeds in the North and East directions in a Cartesian coordinate system. Note that the wind direction in the polar coordinate system is clockwise positive from the North direction. It is seen that the pattern of wind speed and direction records are different for different hurricanes, which depends on a number of factors, including the 7 parameters defining the hurricane eye tracks and wind fields. While the impacts of the hurricane wind field as shown in Fig. 2 on the wind records is complex, a qualitative analysis of the impact of hurricane eye tracks on the wind records provides examples of the range of loading developed during hurricanes. Specifically, when the location of interest is very close to the hurricane eye track, the record of the absolute values of the wind speeds usually has two peaks and the drop of the wind speed in the middle is due to the near zero wind speed in the hurricane eye (see Fig. 3(c)). On the contrary, if the location of interest is further from the hurricane eye track, the record of the absolute values of the wind speeds will typically only have one peak (see Fig. 4(c) and Fig. 5(c)). The difference between Fig. 4 and Fig. 5 is that the hurricane eye passes by the West or East side of the location of interest, which dominates the variation of the wind directions as presented in these two figures.

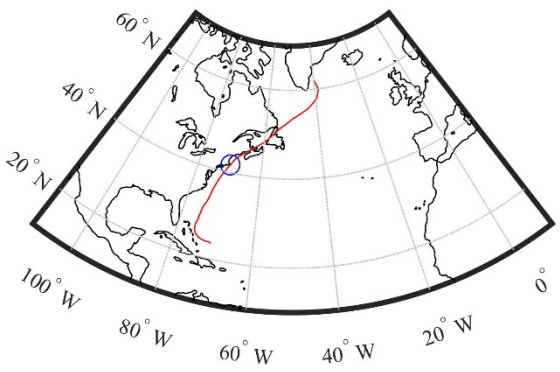

(a) The whole hurricane track (the blue circle represents the 250 km limit)

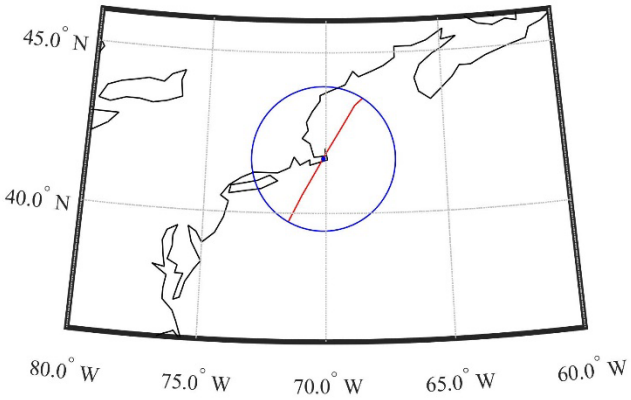

(b) The hurricane track within the 250 km limit (blue circle) of the location of interest (blue dot)

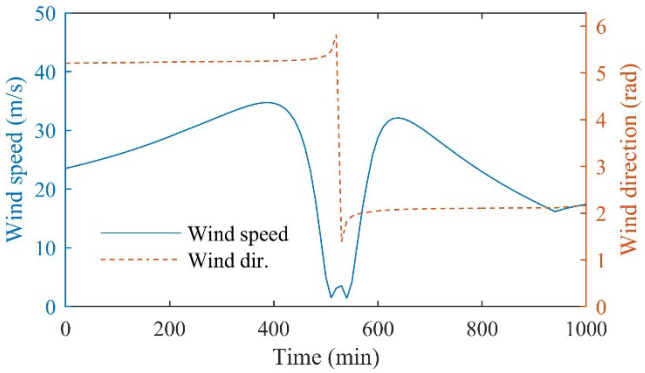

(c) Wind speed and direction records

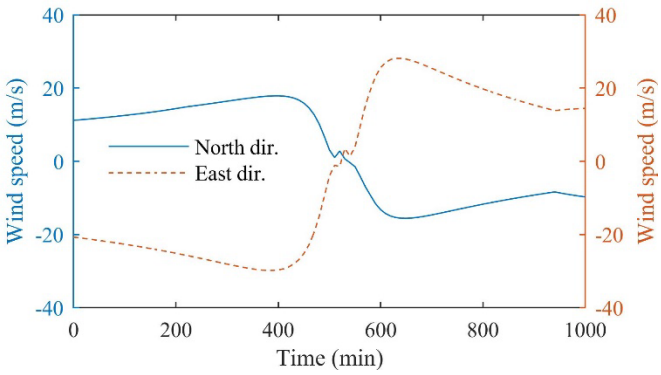

(d) Wind speed records in the North and East directions

Fig. 3. An example of hurricanes going through the location of interest

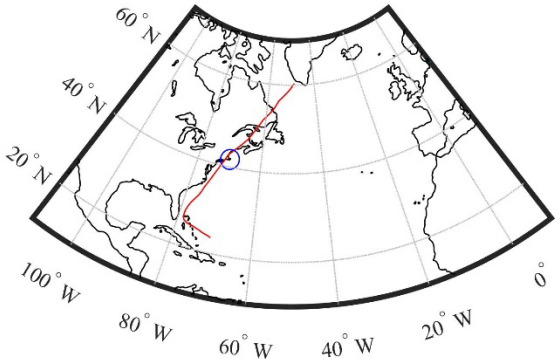

(a) The whole hurricane track (the blue circle represents the 250 km limit)

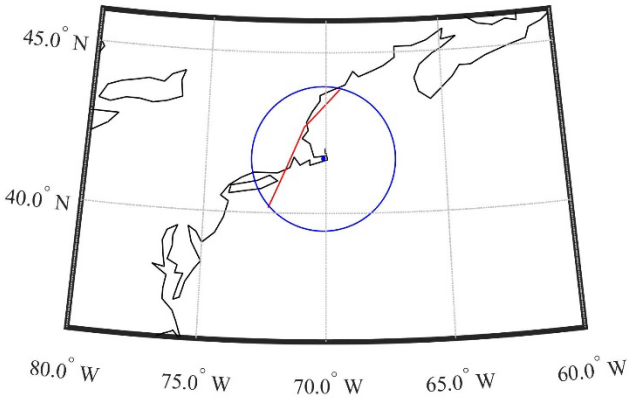

(b) The hurricane track within the 250 km limit (blue circle) of the location of interest (blue dot)

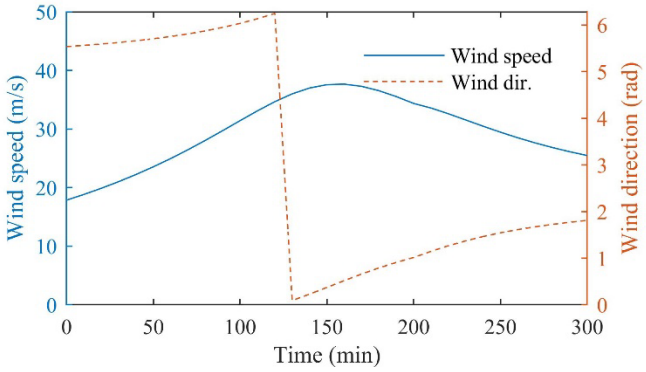

(c) Wind speed and direction records

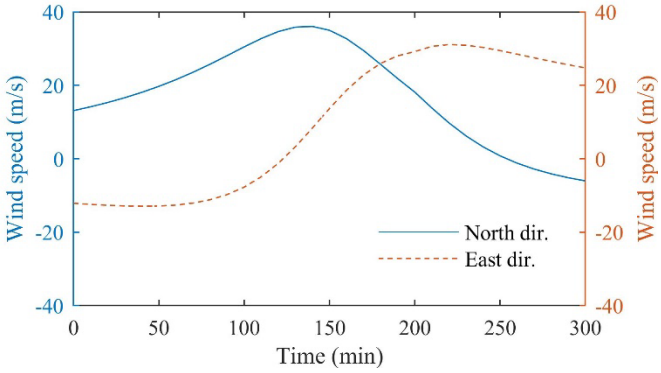

(d) Wind speed records in the North and East directions

Fig. 4. An example of hurricanes passing by the West side of the location of interest

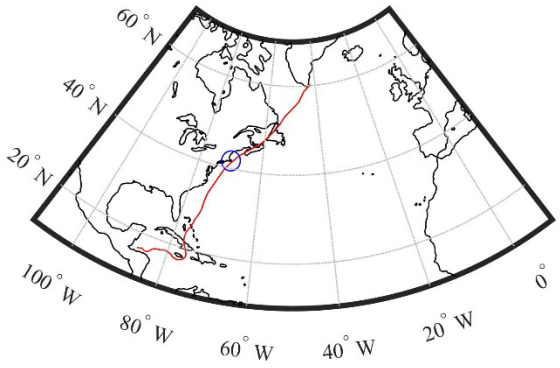

(a) The whole hurricane track (the blue circle represents the 250 km limit)

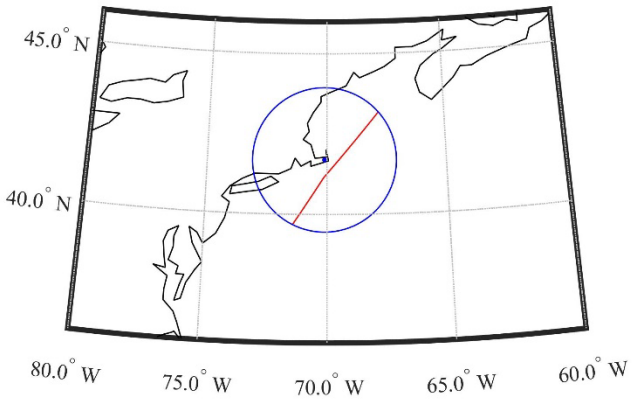

(b) The hurricane track within the 250 km limit (blue circle) of the location of interest (blue dot)

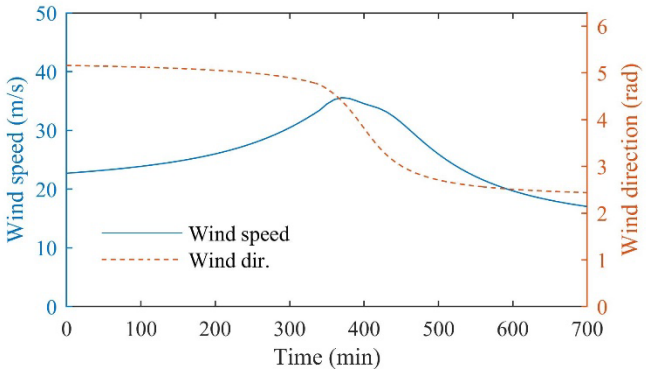

(c) Wind speed and direction records

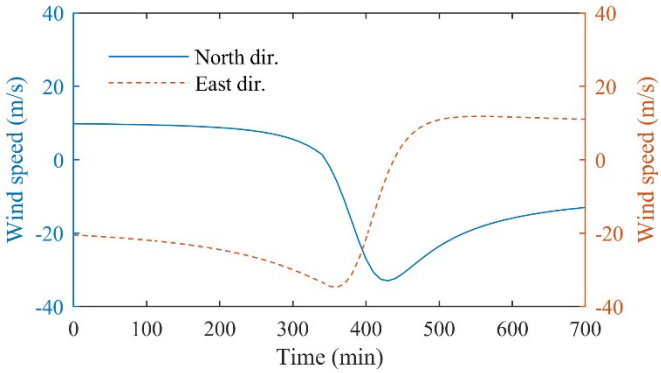

(d) Wind speed records in the North and East directions

Fig. 5. An example of hurricanes passing by the East side of the location of interest

Wind records are first collected through applying the 250 km distance limit between the hurricane eye and the location of interest. Hurricanes with very low wind speeds are then filtered out through a strategy that only hurricanes whose maximum wind speeds at the location of interest are greater than the 50-year MRI wind speed at the same location are considered. The 50-year MRI wind speed obtained from the ASCE 7 Hazard Tool (ASCE, 2016) is a 3-second gust wind speed at 10 m above ground (47 m/s for this location),

231 which is then converted to 10-min sustained wind speed at 10 m above ground (32.4 m/s for this location)
232 following the approach proposed by Simiu and Scanlan (Simiu and Scanlan, 1996). This 50-year MRI 10-
233 min sustained wind speed is used as the threshold for comparison with the collected hurricane wind records
234 to get rid of those with small maximum wind speeds. Thus, a total of 162 hurricane wind records are
235 collected from the 10,000-year synthetic hurricanes, of which 160 records are shown in Fig. 6 within a
236 Cartesian coordinate system and are used in the following sections for clustering. Only 160 records are
237 included because 162 cannot be divided by the batch size (i.e., 16) employed in the training process of the
238 autoencoder, as will be introduced in Section 4.1. In addition, Fig. 7 presents the histogram of the durations
239 of all of the collected hurricanes with a mean duration of 12.4 hours. To avoid the impulse effects, a 1-hour
240 linear ramp-up and a 1-hour linear ramp-down are attached to the beginning and the end of the collected
241 wind records, respectively, as recommended in the Prestandard for Performance-Based Wind Design
242 (ASCE, 2019). To be consistent with the hurricane wind records with 10-min intervals, the ramp is added
243 as six 10-min steps with a constant wind direction. Note that the ramps are not included in Fig. 3 to Fig. 5
244 but included in Fig. 6 and Fig. 7. Moreover, as will be discussed in the following sections, the collected
245 wind records may have different durations, but the autoencoder needs the same size for the input data of
246 each record. Therefore, to facilitate training the autoencoder, zero paddings are added to the beginning and
247 the end of the records that are shorter than the longest one. Consequently, all records after preprocess have
248 the same length as the longest one. For each record, zero paddings at the beginning and the end have the
249 same length, which means all records after preprocessing have a midpoint that is usually recorded when the
250 hurricane eye is closest to the location of interest.

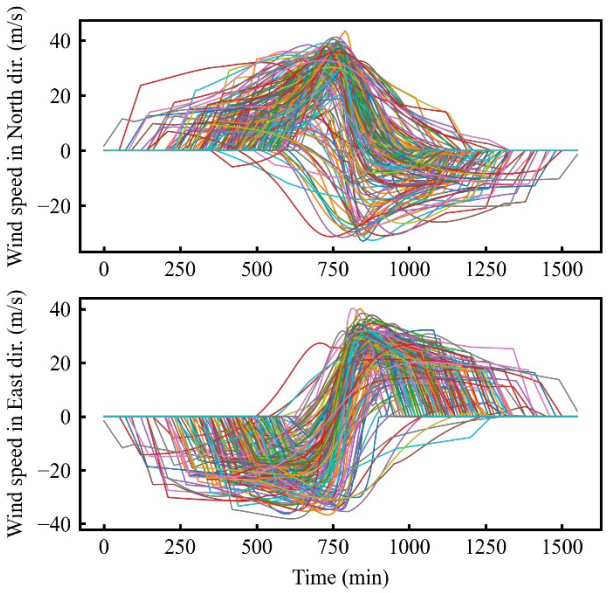

251
252 Fig. 6. The 160 collected hurricane wind records resolved in two directions

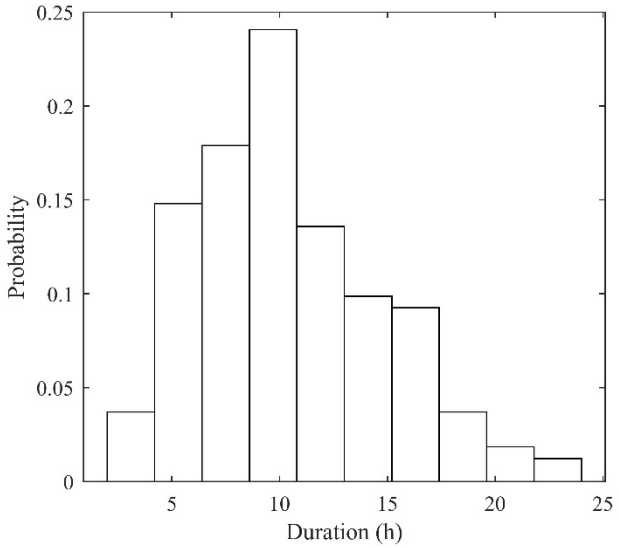

Fig. 7. Histogram of the durations of the collected hurricane wind records

3.2. Wind records for a region

Hurricane wind records for different locations have different patterns. Consequently, it is appropriate to select site-specific wind records instead of generic wind records for all locations. Compared to generic wind records, site-specific wind records have lower uncertainties and thus can be used to predict responses of structures at a given location more accurately. To collect and select site-specific hurricane wind records for a region of interest, this research proposes that this region can be discretized into a set of grids and the centroid of each grid is used to represent the whole grid for recording wind speeds and directions. Thus, hurricane wind records can be collected for all centroids of the grids. To demonstrate this idea, Fig. 8 shows Massachusetts as a testbed, which is divided into 0.2° by 0.2° grids. In Fig. 8, the red dots represent the centroids of the grids that are not associated with Massachusetts, while the 92 blue dots represent the centroids of the grids that are associated with Massachusetts. The hurricane wind records collection procedure proposed in Section 3.1 is then run for all 92 grids. Note that when generating the wind records, the percentage of the sea-land transition defined in Section 2 is calculated for the centroid of each grid based on its fetch distance. In addition, the 50-year MRI wind speeds for the centroids of some grids cannot be obtained from the ASCE 7 Hazard Tool because these centroids are over the ocean (see Fig. 8); therefore, for these cases, locations within the same grids but on the land are used to find the 50-year MRI wind speeds. Figure 9 presents the histogram of the number of hurricanes collected for all 92 grids, with a mean value of 202.

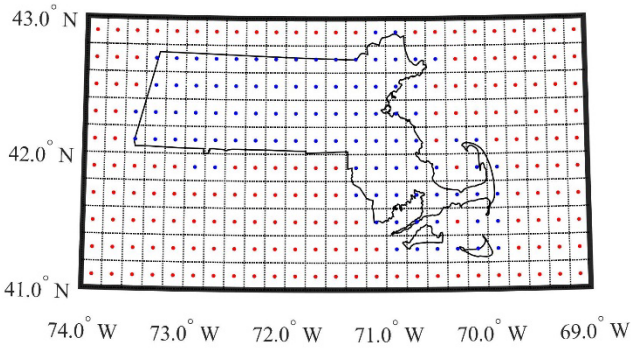

Fig. 8. Massachusetts is discretized into grids

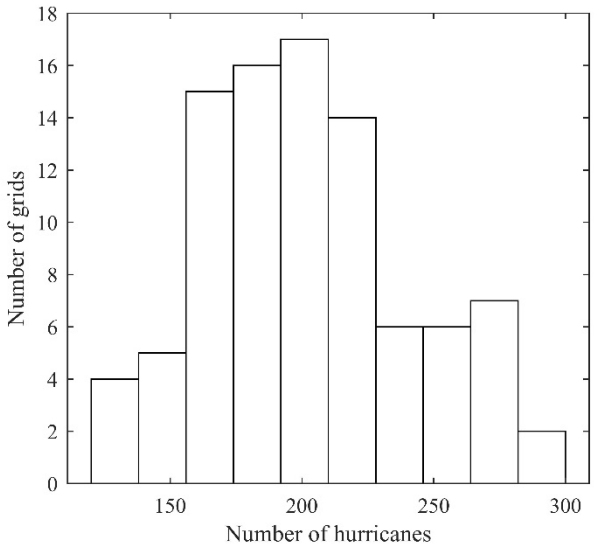

Fig. 9. Histogram of the number of collected hurricanes for the 92 grids

4. Wind records clustering and selection

The approximately 200 collected hurricane wind records for each grid are still too many for design checks and fragility development, especially considering the long durations of the wind records. Incremental dynamic analysis (IDA) may be used to estimate collapse probability of structures under hurricanes (Du et al., 2022; Vamvatsikos and Cornell, 2002). This approach is computationally intensive because direct integration of the nonlinear dynamic governing equations is required over the entire duration of the hurricane wind records and this nonlinear time history analysis needs to be run multiple times with scaled wind records. As such, it is important to limit the number of records used. Therefore, in this research, the collected wind records for each grid are first clustered using a machine learning approach and then approximately 1/10 of the wind records in each cluster are selected, which are combined together to create approximately 20 selected wind records for each grid. This significantly reduces the number of nonlinear

time history analyses required, while still preserving the uncertainties in the collected records. This procedure is similar to stratified sampling in statistics. Sampling is the process of selecting a subset from a population so that the characteristics of the whole population can be estimated using this subset, while stratified sampling is used by dividing the population into subpopulations (i.e., clusters in this paper), where the elements within each subpopulation are similar, and performing sampling on each subpopulation. Stratified sampling may improve the precision of the sample because sampling variability within each subpopulation is smaller than the sampling variability on the entire population (Botev and Ridder, 2017; Parsons, 2014). Specifically, the selected wind records can cover a spread of properties such as durations, patterns of wind speed records, and patterns of wind direction records, because the collected wind records are divided into clusters based on these properties.

4.1. Fully connected autoencoder

Since the collected hurricane wind records are time series of both wind speed and direction with different durations, it is challenging to cluster the records directly. To facilitate the clustering process, the high dimensional wind records are first transformed into low dimensional latent features using an artificial neural network named autoencoder (Aggarwal, 2018; Bond et al., 2022; Tavakoli et al., 2020). The architecture of the autoencoder for wind records at the location of interest given in Section 3.1 is presented in Fig. 10. It is seen that the input matrix is the original wind speed records in the Cartesian system, which has two columns with each column representing wind speed time histories in the North and East directions, respectively. The input matrix is first flattened into a vector as the input layer of the fully connected autoencoder and then passed through other hidden layers to reconstruct the data as another vector in the output layer, which is finally reshaped to a matrix as the reconstructed wind speed records in the Cartesian system. Even though the two columns of the input matrix are correlated time series of wind speeds in two directions, this “flatten” and “reshape” process is reasonable because the correlations are considered in the flattened vectors (input and output layers) through the weights of the fully connected layers. In another word, “flatten” and “reshape” only change the appearance of the data while retaining the relationships and correlations of the elements within the data. A fully connected autoencoder means that all the neurons in one layer are connected to all the neurons in the next layer. The autoencoder architecture consists of two parts: the encoder that compresses the high dimensional input data into the small-size latent feature vector, and the decoder that utilizes the latent features to reconstruct the input data. In this example, the flattened wind speeds in the input layer are transformed into 5 latent features through the encoder process, which are then expanded to form the reconstructed but still flattened wind records in the output layer through the decoder process. The hidden layers with a nonlinear activation function (Tanh) are included to enhance the power of this autoencoder so that it can map the input data into much smaller dimensional spaces. Here

Tanh is adopted because it has better performance than other activation functions based on numerical tests in this research. This autoencoder architecture requires that all input matrices have the same size; thus, the size of the longest wind record is used as the size of the input matrices and zero padding is added to the beginning and the end of all other shorter wind records. This strategy retains all information in the wind records. In this example, the longest record has 156 data points (including the ramp-up and ramp-down) with 10-min intervals, so the number of rows of the input matrices is 156.

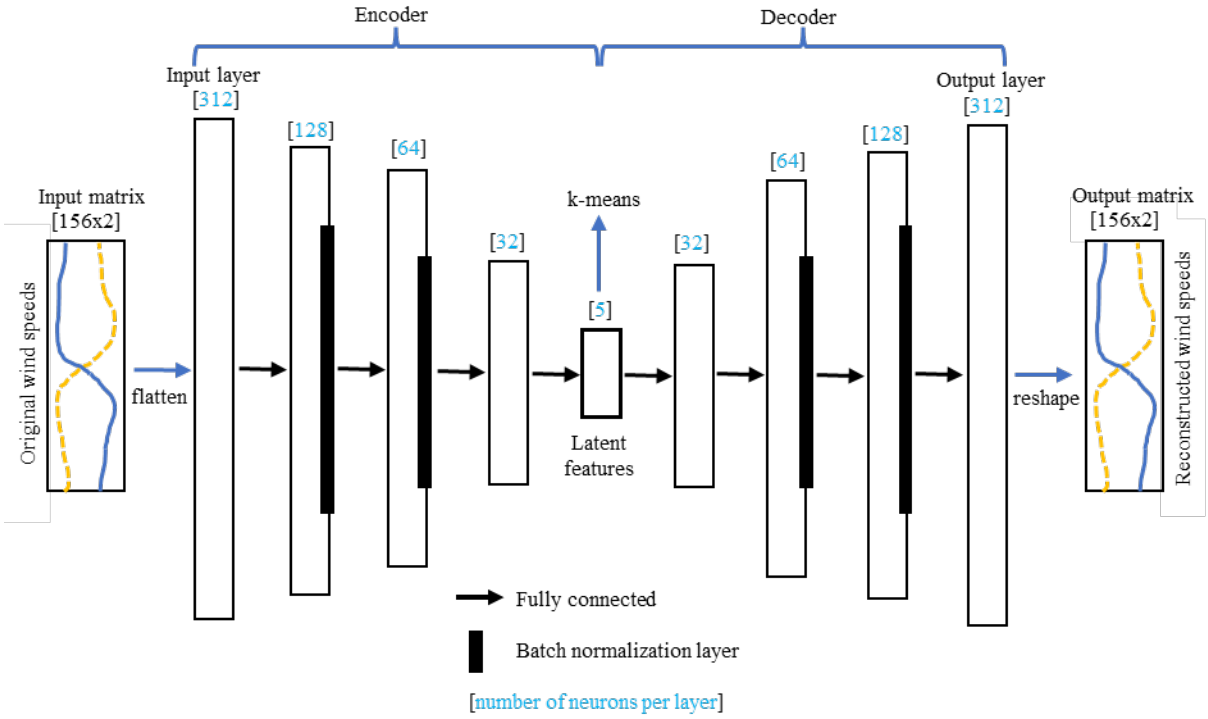

Fig. 10. The proposed autoencoder architecture

The training of this autoencoder is conducted by minimizing the error between the reconstructed data in the output layer and the input data, which ensures that the latent features can represent the important patterns of the wind records. The Adaptive Moment Estimation (Adam) algorithm is adopted for stochastic optimization and batch normalization is added to some hidden layers as shown in Fig. 10 to address the exploding and vanishing gradient problems (Aggarwal, 2018). Since the chosen batch size is 16, only 160 of the collected 162 wind records are used for the training process. In addition, Fig. 11 illustrates the reconstructed 160 wind records in the North and East directions after training the proposed autoencoder neural network. The histogram of the reconstruction error between the original and the reconstructed wind records is shown in Fig. 12, which demonstrates that the reconstructed records match well with the original ones and the latent features hold the most important characteristics of the wind records. It should be noted that since the 312 data points in the input layer is compressed into only 5 latent features, there must be some loss of information in this process and the discrepancies between the original and the reconstructed records

are inevitable. However, these discrepancies are usually induced by noise or other nonsignificant factors; therefore, the low dimensional latent features should be adequate for clustering because the important information has been extracted through the autoencoder.

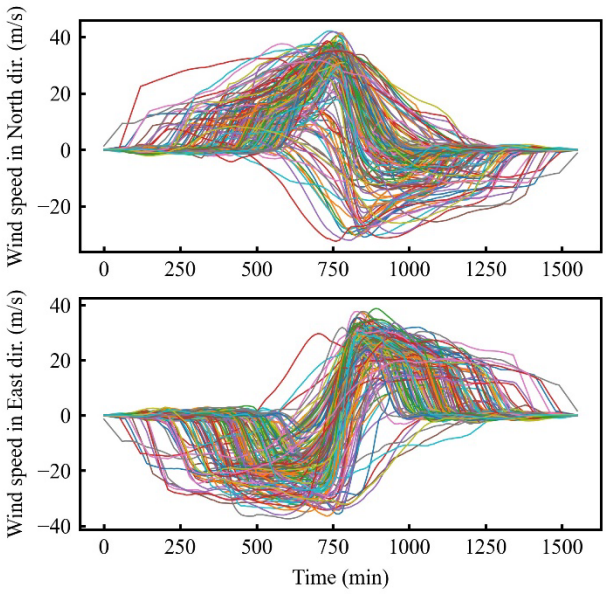

Fig. 11. The 160 reconstructed wind records in two directions for the location of interest

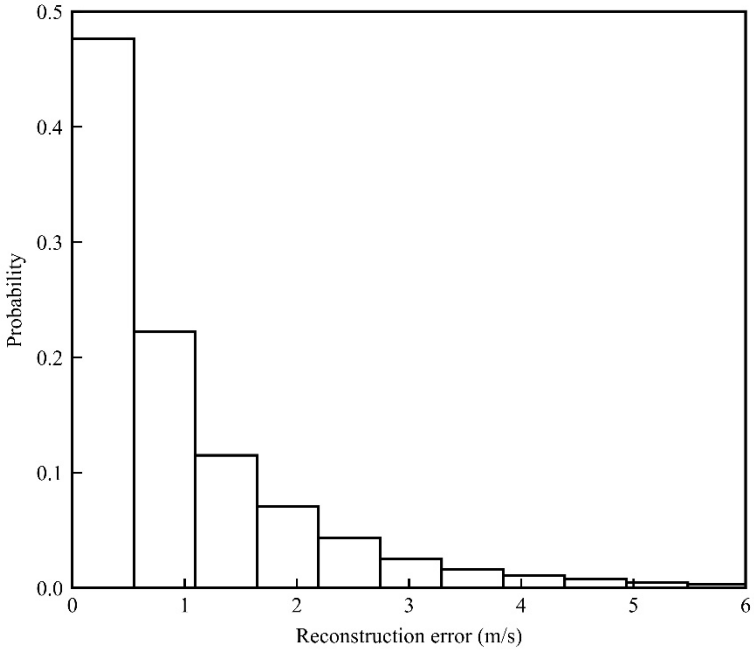

Fig. 12. Histogram of the reconstruction error

4.2. Clustering and selection based on latent features

The location of interest studied in Sections 3.1 and 4.1 is used here as an example. After the training process, all wind speed time series are converted into latent feature vectors, on which the k-means algorithm is applied for clustering. The goal of clustering is to maximize the similarity of data within each cluster and maximize the dissimilarity of data in distinct clusters. Therefore, one can take a subset of the data in a cluster to represent all data in that cluster, the accuracy of which depends on the number of clusters used. Here, the elbow rule is adopted to find an optimal number of clusters (Thorndike, 1953). To do so, the k-means algorithm has been run multiple times on the latent features with different number of clusters ranging from 2 to 20. For this example, when the number of clusters k equals 8, the Within-Cluster-Sum of Squared Errors (WSS) curve reaches its elbow as shown in Fig. 13. Therefore, the 160 hurricane wind records are divided into 8 clusters. Since it is difficult to show the 5 latent features on a 2D or 3D figure, principal component analysis is performed on the latent features and the first 3 principal components are plotted in Fig. 14 to demonstrate the results of the k-means clustering. This is acceptable because the first 3 principal components possess 82% of the variation of the 5 latent features and it is believed that the 5 latent features must show better performance than the 3 principal components if they can be plotted in a figure. In Fig. 14, the first 3 principal components are presented using 8 different colors for the 8 clusters, from which it may be seen that the hurricane wind records are clustered well because the principal components of different clusters have rare overlaps and the principal components of each cluster are gathered closely around their centroid.

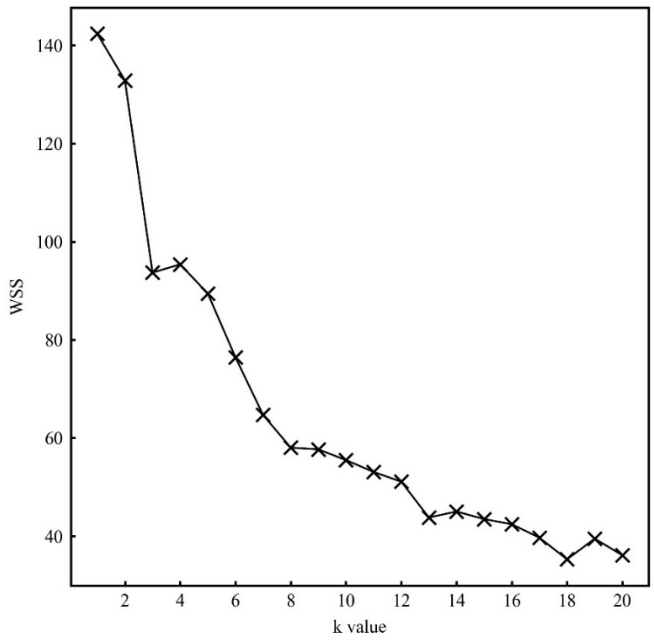

Fig. 13. The WSS for different number of clusters

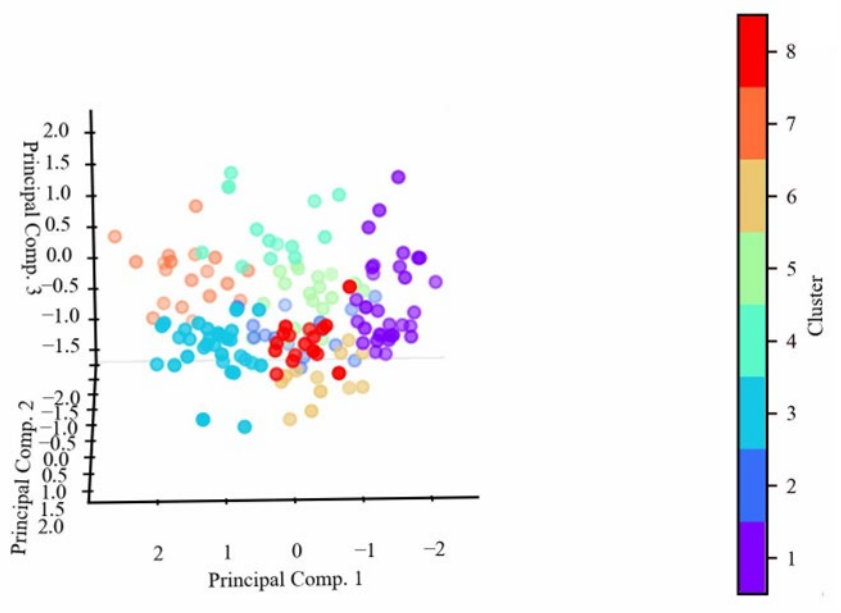

Fig. 14. Principal components of the latent features for the 8 clusters

To demonstrate the effectiveness of the proposed clustering approach, Fig. 15 to Fig. 22 illustrate the hurricane wind speeds and tracks of the 8 clusters. It is seen that the clustering results are successful, because hurricane wind speeds and durations within each cluster have similar patterns. Specifically, Clusters 2 and 7 have hurricanes whose tracks pass by the East side of the location of interest, while other clusters have hurricanes whose tracks pass by the West side of the location of interest. The number of hurricanes in each cluster from Cluster 1 to Cluster 8 are 31, 17, 31, 13, 20, 12, 19 and 17, respectively. So much more hurricanes pass by the West side of the location of interest than the East side. The main difference between Cluster 2 and Cluster 7 is that the durations of hurricanes in Cluster 7 is longer. For the clusters passing by the West side of the location of interest, Cluster 3 and Cluster 4 has the shortest and the longest durations, respectively, while Clusters 1, 5, 6 and 8 have durations in the middle. Clusters 6 and 8 have very similar durations, but they are divided into two clusters because they have different shapes for the profile of the wind speed time histories. There are outliers in some clusters such as the one with abrupt changing of the storm heading direction as seen in the figure of hurricane tracks of Cluster 2. This can be expected because the k-means algorithm cannot eliminate all outliers, but instead assigns outliers to their closest cluster. Usually, outliers are rare and their latent feature points are far from the centroid of all points in a cluster. Therefore, the outlier commonly will not be included to the final suite of wind records considering the selection strategy within a cluster that will be introduced below. The wind field shown in Fig. 2 also has impacts on the clustering results, which cannot be explained explicitly here because its information is included in the latent features through the operations on the wind records during the training of the autoencoder.

Considering the computational demand of nonlinear time-history analyses that these wind records will be used to perform, approximately 1/10 of the hurricanes in each cluster are selected and combined together as the final suite of hurricane wind records. The number of records selected from each cluster is proportional to the total number of records in each cluster, which results in 3, 2, 3, 1, 2, 1, 2 and 2 records from each cluster, respectively. This strategy is used to make sure the proportions of different patterns of wind records are similar in the selected 16 hurricanes and the original 160 ones. It is also reasonable to make sure the selected records from each cluster are the most representative ones. To achieve this goal, the clustering results of the latent features are used, and for each cluster it is recommended to select those records whose latent feature points are the closest to the centroid of all latent feature points in that cluster. The selected records for each cluster are highlighted in bold solid lines as shown in Fig. 15(a) to Fig. 22(a), which is a demonstration of the validity of this selection strategy within a cluster. In Fig. 15(a) to Fig. 22(a), all wind records are shown in different colors and curves resolved from the same record are shown in the same color in the upper subplot and lower subplot. It is seen that the selected records are representative, as they are near the middle of all the records. The total of 16 selected hurricanes can be employed to represent uncertainties in wind loading for design check and fragility development for structures at the location of interest. Note that these selected wind records are only time series of 10-min mean wind speed at 10 meters height. If one wants to use them for structural dynamic analysis, the fluctuating wind speeds and the atmospheric boundary layer should be considered.

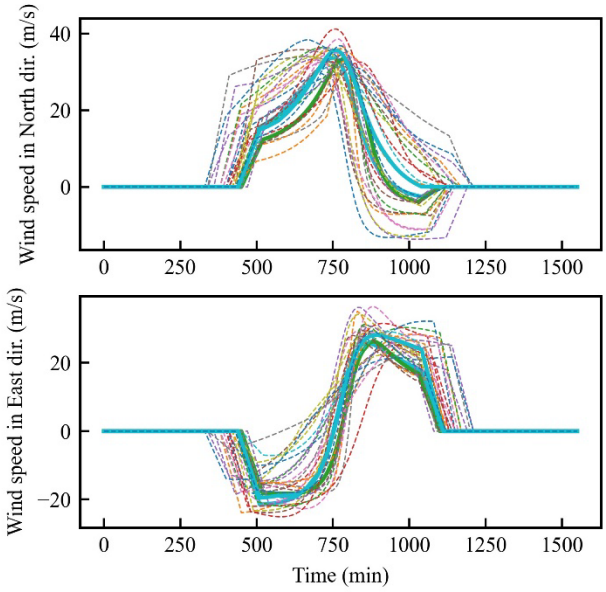

(a) Wind records of Cluster 1

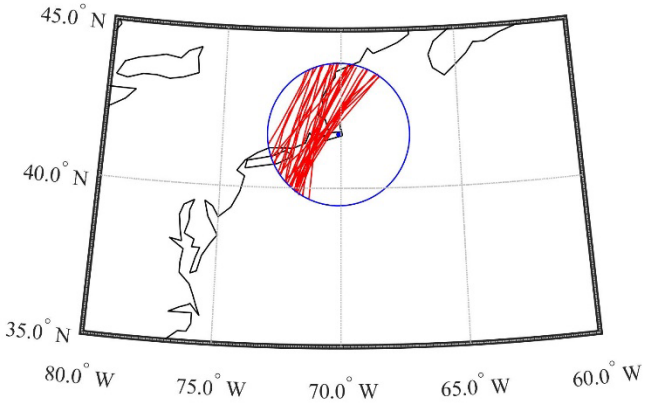

(b) Hurricane eye tracks of Cluster 1

Fig. 15. Hurricanes in Cluster 1

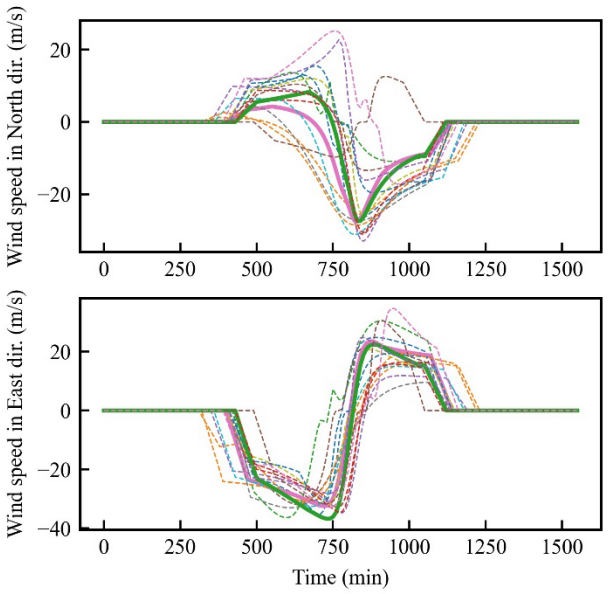

(a) Wind records of Cluster 2

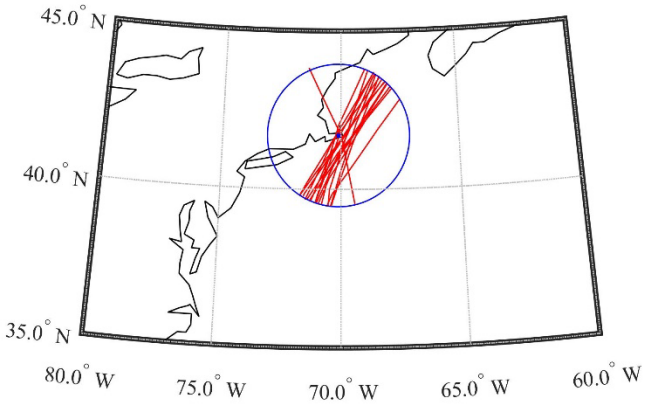

(b) Hurricane eye tracks of Cluster 2

Fig. 16. Hurricanes in Cluster 2

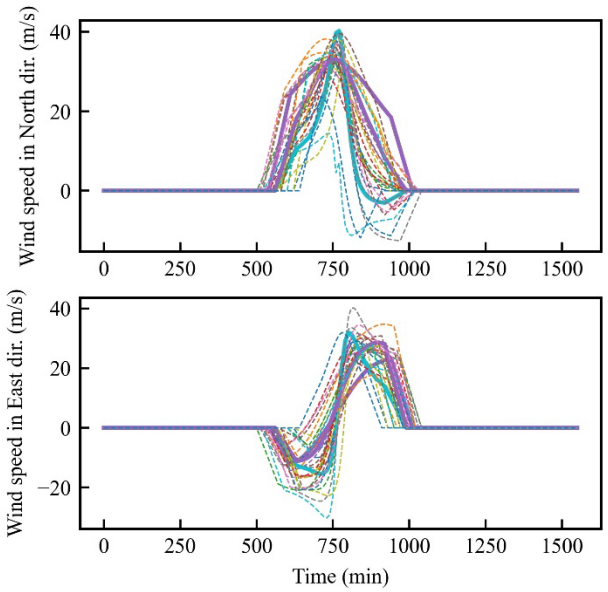

(a) Wind records of Cluster 3

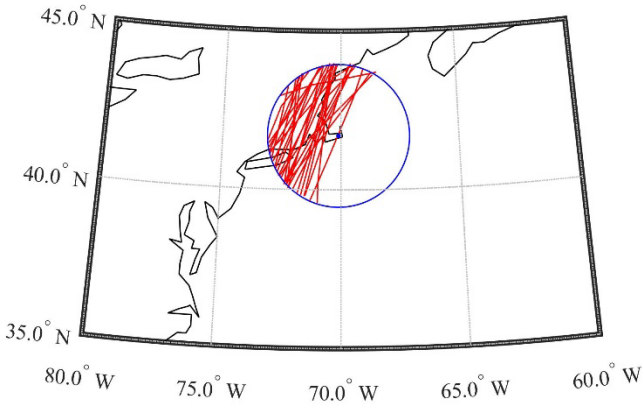

(b) Hurricane eye tracks of Cluster 3

Fig. 17. Hurricanes in Cluster 3

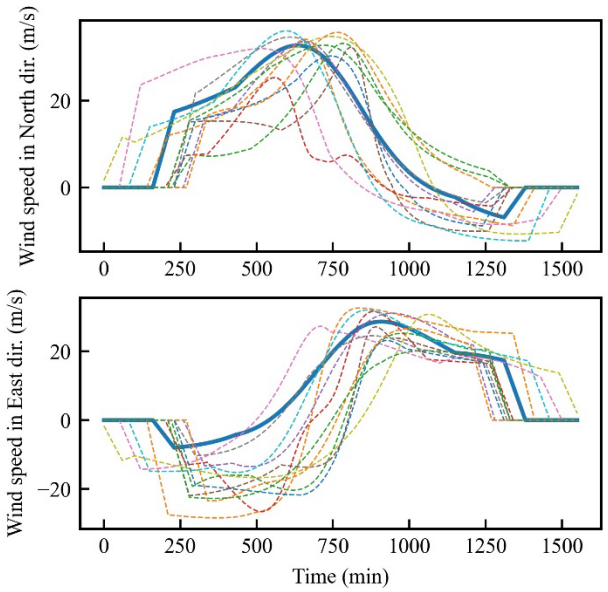

(a) Wind records of Cluster 4

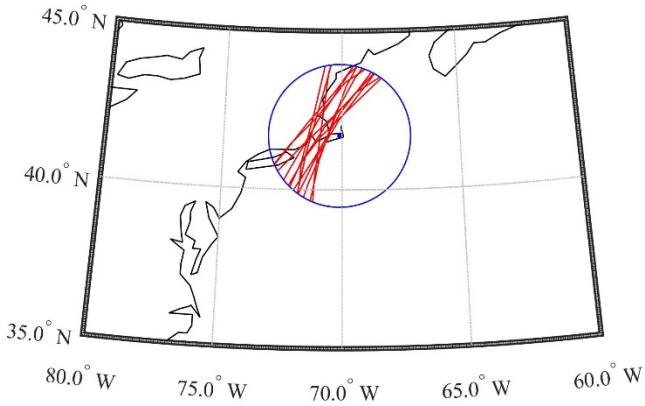

(b) Hurricane eye tracks of Cluster 4

Fig. 18. Hurricanes in Cluster 4

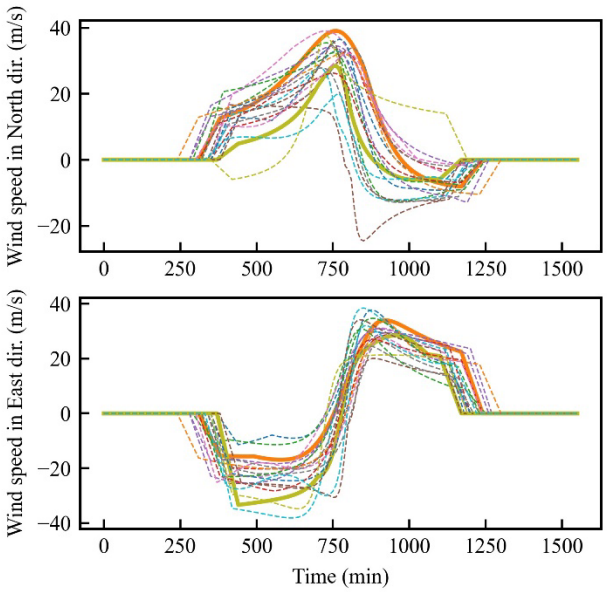

(a) Wind records of Cluster 5

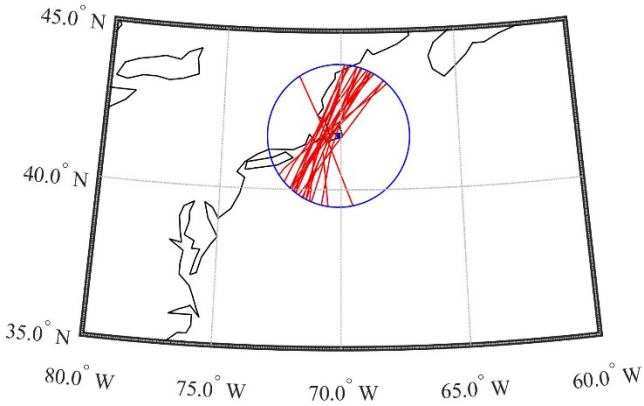

(b) Hurricane eye tracks of Cluster 5

Fig. 19. Hurricanes in Cluster 5

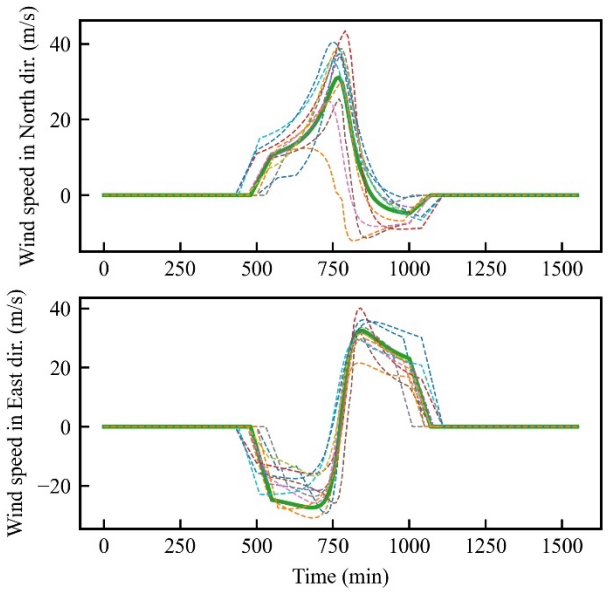

(a) Wind records of Cluster 6

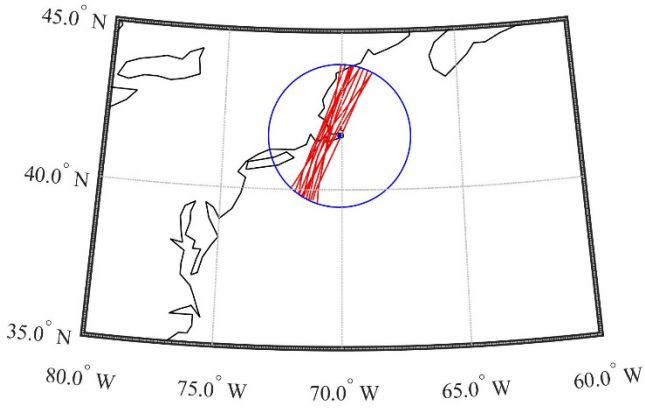

(b) Hurricane eye tracks of Cluster 6

Fig. 20. Hurricanes in Cluster 6

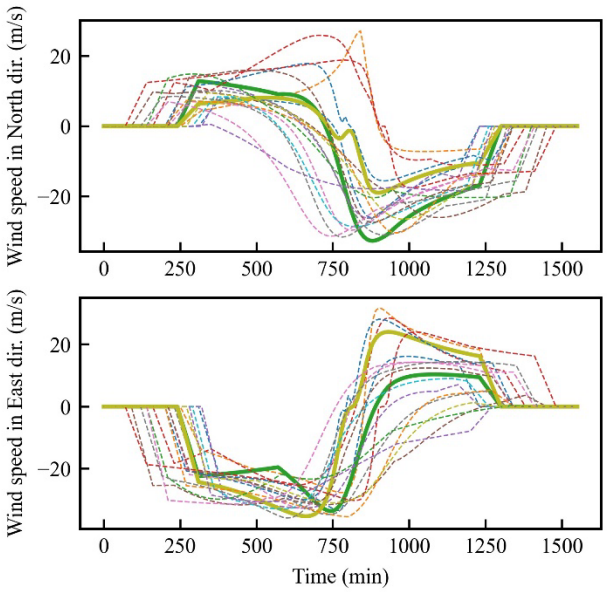

(a) Wind records of Cluster 7

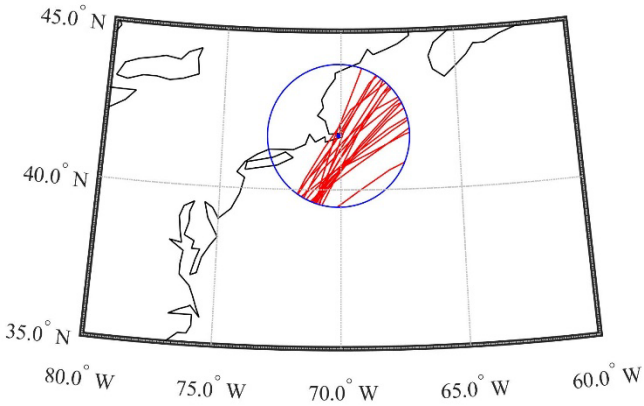

(b) Hurricane eye tracks of Cluster 7

Fig. 21. Hurricanes in Cluster 7

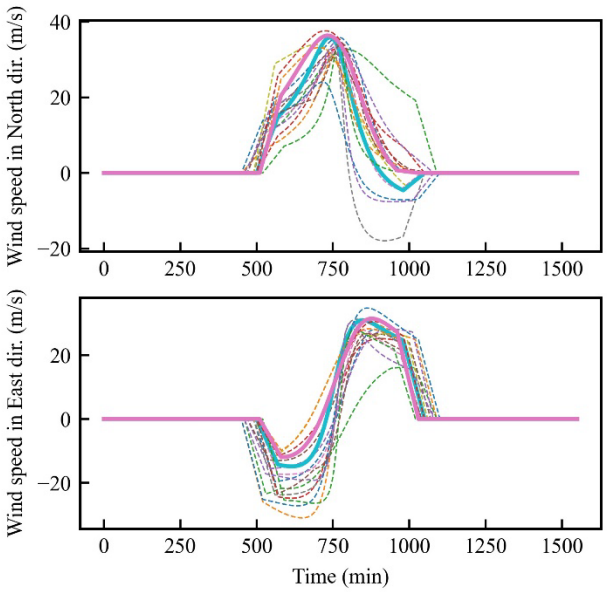

(a) Wind records of Cluster 8

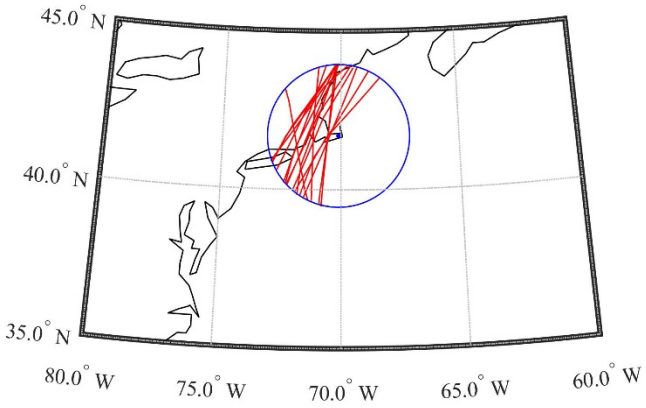

(b) Hurricane eye tracks of Cluster 8

Fig. 22. Hurricanes in Cluster 8

4.3. Wind records selection for a region

As a case study for regional analysis, Massachusetts has been divided into 92 girds and wind records has been collected for each grid given in Section 3.2. Here the procedures for wind records clustering and selection introduced in Sections 4.1 and 4.2 are applied to all 92 grids. The same autoencoder architecture is used for all grids except for the slightly different sizes of the input vectors for different grids, which is because the maximum duration of the collected records for different grids may be different. The same k-means algorithm is also adopted for clustering on the latent features; however, the number of clusters may vary for different grids because it is dynamically determined using the elbow rule. The histogram of the number of clusters for all grids is presented in Fig. 23 with a mean value of 5.65. Since approximately 200 hurricane wind records are collected for each grid, then approximately 20 records are selected for each grid

according to the method introduced in Section 4.2. Finally, a wind map is generated so that a suite of hurricane wind speed and direction records can be provided for any locations in Massachusetts. For example, Fig. 24(a) gives 16 wind records selected from 8 clusters for a grid whose centroid has a latitude of 41.7 and a longitude of -70.1 (this location is used in Sections 3.1 and 4.1), while Fig. 24(b) gives 19 wind records selected from 4 clusters for a grid whose centroid has a latitude of 42.1 and a longitude of -72.5. Here the wind records selected from the same cluster are shown in the same color, and it is seen that wind records within the same cluster have similar characteristics in terms of wind speeds, directions, and durations. This approach provides an alternative to the ASCE 7 wind map. The ASCE 7 wind map can only provide a wind speed without any information of variation of the wind speed and direction during a hurricane. This methodology can be generalized to any other regions besides Massachusetts.

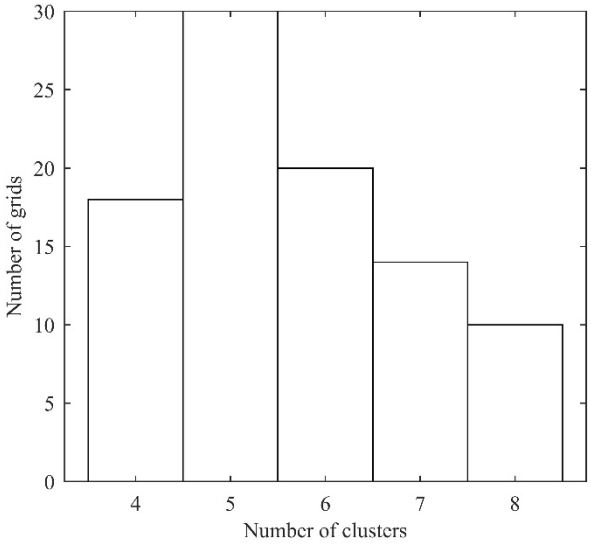

Fig. 23. Histogram of the number of clusters for all grids

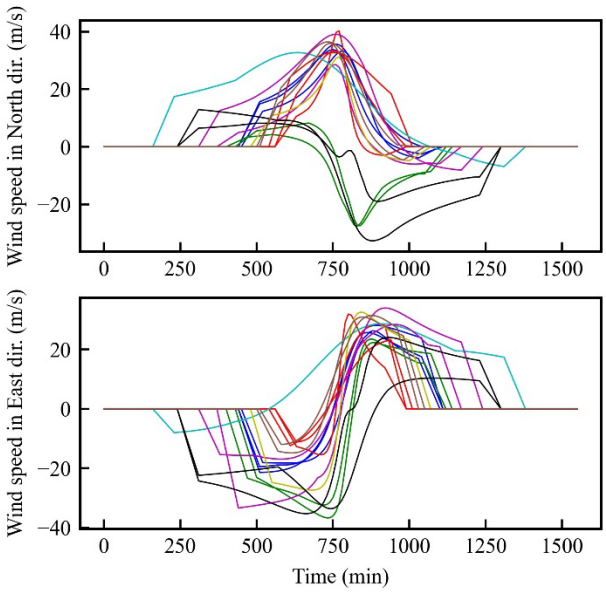

(a) For a grid whose centroid has a latitude of 41.7 and a longitude of -70.1

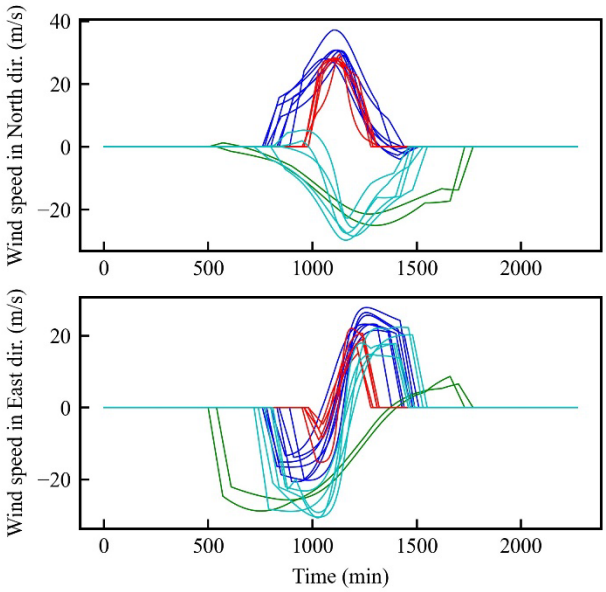

(b) For a grid whose centroid has a latitude of 42.1 and a longitude of -72.5

Fig. 24. Examples of selected hurricane wind records

5. Conclusions

This paper presents a machine learning approach for collecting and selecting hurricane wind speed and direction records for a location and a region, which can be used for efficiently developing fragility curves or assessing probabilistic behaviors of structures considering uncertainties in hurricanes. The selected hurricane wind records are supposed to address the uncertainties in hurricanes because 1) they are selected from 10,000-year synthetic hurricanes and 2) the collected records with similar properties are first divided

into clusters and then the most representative ones are selected from each cluster. The preprocess of the wind records is also important since it can remove hurricanes with very small wind speeds and limit the durations of the records to a relatively short time. The proposed autoencoder architecture is shown to be able to reconstruct the wind speed time series and compress them into low dimensional latent features. The clustering results based on the latent features using the k-means algorithm are successful, because the points in the latent space are divided clearly into several clusters, and the wind records in the same cluster exhibit similar properties in duration, hurricane track, and changing of wind speed and directions. A method is also proposed to select the most representative records from each cluster based on the clustering results of latent features. This hurricane selection procedure is demonstrated using wind records from both a location and a region. For the regional hurricane selection, Massachusetts is used as a testbed, and it is discretized into a set of grids with performing the proposed hurricane selection procedure on each grid. Usually, approximate 20 wind records are selected for a location, which make the nonlinear structural analysis feasible for uncertainty propagation simulation under hurricanes.

Acknowledgement

The authors wish to thank Dr. Weichiang Pang of Clemson University for providing the synthetic hurricane catalog. The material presented in this paper is based upon work supported by National Science Foundation under Grant No. CRISP-1638234 and Northeastern University. This support is gratefully acknowledged.

References

Aggarwal, C. C. (2018). *Neural networks and deep learning*. Yorktown Heights, NY: Springer International Publishing AG, part of Springer Nature.

Aggarwal, C. C., Hinneburg, A., and Keim, D. A. (2001). *On the surprising behavior of distance metrics in high dimensional space.* Paper presented at the International conference on database theory.

ASCE. ASCE 7 Hazard Tool. Retrieved from https://asce7hazardtool.online/.

ASCE. (2016). Minimum Design Loads and associated criteria for Buildings and Other Structures (ASCE Standard 7-16). In. Reston, VA: American Society of Civil Engineers.

ASCE. (2019). Prestandard for Performance-Based Wind Design. In. Reston, VA: American Society of Civil Engineers.

Baker, J. W., and Lee, C. (2018). An improved algorithm for selecting ground motions to match a conditional spectrum. *Journal of Earthquake Engineering, 22*(4), 708-723.

Barbato, M., Petrini, F., Unnikrishnan, V. U., and Ciampoli, M. (2013). Performance-based hurricane engineering (PBHE) framework. *Structural Safety, 45*, 24-35.

Batts, M. E., Cordes, M. R., Russell, L. R., Shaver, J. R., and Simiu, E. (1980). *Hurricane wind speeds in the United States*. (0044-8001).

Bojórquez, E., Reyes-Salazar, A., Ruiz, S. E., and Bojórquez, J. (2013). A New Spectral Shape-Based Record Selection Approach Using and Genetic Algorithms. *Mathematical Problems in Engineering, 2013*.

Bond, R. B., Ren, P., Hajjar, J. F., and Sun, H. (2022). AN UNSUPERVISED MACHINE LEARNING APPROACH FOR GROUND MOTION CLUSTERING AND SELECTION. *Earthquake Spectra*. (under review).

519 Botev, Z., and Ridder, A. (2017). Variance reduction. *Wiley StatsRef: Statistics Reference Online*, 1-6.
520 Chuang, W.-C., and Spence, S. M. (2019). An efficient framework for the inelastic performance assessment
521 of structural systems subject to stochastic wind loads. *Engineering Structures, 179*, 92-105.
522 Chuang, W.-C., and Spence, S. M. (2020). Probabilistic performance assessment of inelastic wind excited
523 structures within the setting of distributed plasticity. *Structural Safety, 84*, 101923.
524 Cui, W., and Caracoglia, L. (2015). Simulation and analysis of intervention costs due to wind-induced
525 damage on tall buildings. *Engineering Structures, 87*, 183-197.
526 Cui, W., and Caracoglia, L. (2019). A new stochastic formulation for synthetic hurricane simulation over
527 the North Atlantic Ocean. *Engineering Structures, 199*, 109597.
528 Der Kiureghian, A. (2005). First-and second-order reliability methods. *Engineering design reliability*
529 *handbook, 14*.
530 Du, A., and Padgett, J. E. (2021). Refined multivariate return period-based ground motion selection and
531 implications for seismic risk assessment. *Structural Safety, 91*, 102079.
532 Du, X., and Hajjar, J. F. (2022). *Nonlinear dynamic analysis and fragility development of electrical*
533 *transmission towers under hurricanes*. Paper presented at the Annual Stability Conference,
534 Denver, CO.
535 Du, X., Hajjar, J. F., Bond, R. B., and Sun, H. (2022). *Collapse fragility development of electrical transmission*
536 *towers subjected to hurricanes*. Paper presented at the IABSE Symposium Prague 2022, Challenges
537 for Existing and Oncoming Structures, Prague, Czech Republic.
538 FEMA. (2009). Quantification of building seismic performance factors. In *FEMA-P695*: Federal Emergency
539 Management Agency.
540 Georgiou, P. N. (1985). *Design wind speeds in tropical cyclone-prone regions.* (PhD Dissertation). University
541 of Western Ontario, London, Ontario, Canada.
542 Hallowell, S. T., Myers, A. T., Arwade, S. R., Pang, W., Rawal, P., Hines, E. M., . . . Wei, K. (2018). Hurricane
543 risk assessment of offshore wind turbines. *Renewable Energy, 125*, 234-249.
544 Holland, G. J. (1980). An analytic model of the wind and pressure profiles in hurricanes. *Monthly weather*
545 *review, 108*(8), 1212-1218.
546 Jarvinen, B. R., Neumann, C. J., and Davis, M. A. (1984). *A tropical cyclone data tape for the North Atlantic*
547 *Basin, 1886-1983: Contents, limitations, and uses*. Washington, D.C.
548 Jayaram, N., Lin, T., and Baker, J. W. (2011). A computationally efficient ground-motion selection
549 algorithm for matching a target response spectrum mean and variance. *Earthquake Spectra, 27*(3),
550 797-815.
551 Joyner, M. D., and Sasani, M. (2018). Multihazard Risk-Based Resilience Analysis of East and West Coast
552 Buildings Designed to Current Codes. *Journal of structural engineering, 144*(9), 04018156.
553 Kim, S.-M., Ok, S.-Y., and Song, J. (2019). Multi-scale dynamic system reliability analysis of actively-
554 controlled structures under random stationary ground motions. *KSCE Journal of Civil Engineering,*
555 *23*(3), 1259-1270.
556 Kim, T., Kwon, O. S., and Song, J. (2021). Clustering‐based adaptive ground motion selection algorithm for
557 efficient estimation of structural fragilities. *Earthquake Engineering & Structural Dynamics, 50*(6),
558 1755-1776.
559 Krawinkler, H., Medina, R., and Alavi, B. (2003). Seismic drift and ductility demands and their dependence
560 on ground motions. *Engineering Structures, 25*(5), 637-653.
561 Li, Y. (2005). *Fragility methodology for performance-based engineering of wood-frame residential*
562 *construction.* (PhD Dissertation). Georgia Institute of Technology, Atlanta, GA.
563 Li, Y., and Ellingwood, B. R. (2006). Hurricane damage to residential construction in the US: Importance of
564 uncertainty modeling in risk assessment. *Engineering Structures, 28*(7), 1009-1018.

Liu, F. (2014). *Projections of future US design wind speeds and hurricane losses due to climate change.* (PhD Dissertation). Clemson University, Clemson, SC.
Ma, L., Khazaali, M., and Bocchini, P. (2021). Component-based fragility analysis of transmission towers subjected to hurricane wind load. *Engineering Structures, 242*, 112586.
Moehle, J., and Deierlein, G. G. (2004). *A framework methodology for performance-based earthquake engineering.* Paper presented at the 13th world conference on earthquake engineering.
Naeim, F., Alimoradi, A., and Pezeshk, S. (2004). Selection and scaling of ground motion time histories for structural design using genetic algorithms. *Earthquake Spectra, 20*(2), 413-426.
Parsons, V. L. (2014). Stratified sampling. *Wiley StatsRef: Statistics Reference Online*, 1-11.
Pei, B., Pang, W., Testik, F. Y., Ravichandran, N., and Liu, F. (2014). Mapping joint hurricane wind and surge hazards for Charleston, South Carolina. *Natural hazards, 74*(2), 375-403.
Pei, B., Pang, W., Testik, F. Y., Ravichandran, N., and Liu, F. (2018). Selection of hazard-consistent hurricane scenarios for regional combined hurricane wind and flood loss estimation. *Natural hazards, 91*(2), 671-696.
Russell, L. R. (1971). Probability distributions for hurricane effects. *Journal of the Waterways, Harbors and Coastal Engineering Division, 97*(1), 139-154.
Shalev-Shwartz, S., and Ben-David, S. (2014). *Understanding machine learning: From theory to algorithms*. New York, NY: Cambridge University Press.
Simiu, E., and Scanlan, R. H. (1996). *Wind effects on structures: fundamentals and applications to design* (3rd ed.). New York, NY: John Wiley & Sons, Inc.
Somerville, P., Smith, N., Punyamurthula, S., and Sun, J. (1997). *Development of ground motion time histories for phase 2 of the FEMA/SAC steel project*. Richmond, CA: SAC Joint Venture.
Straub, D., Schneider, R., Bismut, E., and Kim, H.-J. (2020). Reliability analysis of deteriorating structural systems. *Structural Safety, 82*, 101877.
Tabbuso, P., Spence, S. M., Palizzolo, L., Pirrotta, A., and Kareem, A. (2016). An efficient framework for the elasto-plastic reliability assessment of uncertain wind excited systems. *Structural Safety, 58*, 69-78.
Tavakoli, N., Siami-Namini, S., Khanghah, M. A., Soltani, F. M., and Namin, A. S. (2020). An autoencoder-based deep learning approach for clustering time series data. *SN Applied Sciences, 2*(5), 1-25.
Thorndike, R. L. (1953). Who belongs in the family? *Psychometrika, 18*(4), 267-276.
Vamvatsikos, D., and Cornell, C. A. (2002). Incremental dynamic analysis. *Earthquake Engineering & Structural Dynamics, 31*(3), 491-514.
Vickery, P., Skerlj, P., and Twisdale, L. (2000a). Simulation of hurricane risk in the US using empirical track model. *Journal of structural engineering, 126*(10), 1222-1237.
Vickery, P. J., Masters, F. J., Powell, M. D., and Wadhera, D. (2009a). Hurricane hazard modeling: The past, present, and future. *Journal of Wind Engineering and Industrial Aerodynamics, 97*(7-8), 392-405.
Vickery, P. J., Skerlj, P., Steckley, A., and Twisdale, L. (2000b). Hurricane wind field model for use in hurricane simulations. *Journal of structural engineering, 126*(10), 1203-1221.
Vickery, P. J., Skerlj, P. F., Lin, J., Twisdale Jr, L. A., Young, M. A., and Lavelle, F. M. (2006). HAZUS-MH hurricane model methodology. II: Damage and loss estimation. *Natural Hazards Review, 7*(2), 94-103.
Vickery, P. J., Wadhera, D., Galsworthy, J., Peterka, J. A., Irwin, P. A., and Griffis, L. A. (2010). Ultimate wind load design gust wind speeds in the United States for use in ASCE-7. *Journal of structural engineering, 136*(5), 613-625.
Vickery, P. J., Wadhera, D., Powell, M. D., and Chen, Y. (2009b). A hurricane boundary layer and wind field model for use in engineering applications. *Journal of Applied Meteorology and Climatology, 48*(2), 381-405.

612 Vickery, P. J., Wadhera, D., Twisdale Jr, L. A., and Lavelle, F. M. (2009c). US hurricane wind speed risk and
613 uncertainty. *Journal of structural engineering, 135*(3), 301-320.
614 Wang, H., and Wu, T. (2022). Statistical investigation of wind duration using a refined hurricane track
615 model. *Journal of Wind Engineering and Industrial Aerodynamics, 221*, 104908.
616 Zhang, R., Hajjar, J., and Sun, H. (2020). Machine learning approach for sequence clustering with
617 applications to ground-motion selection. *Journal of engineering mechanics, 146*(6), 04020040.

618